Supplementary Information

Related work

Some dynamic models of the octopus robotic system has been presented in [1]. Among the prototypes presented, PoseiDrone, an octopus like robot shown in Figure S1(a), is made of several equidistant arms with swimming abilities imparted by using jet propulsion. Each arm has its own crank-like actuator that can bend or extend the arm using a sequence of inward movements and releasing of the water from the chamber allowing for maneuvering via crawling or swimming [2,3]. An OctopusGripper, Figure S1(b), is also presented, with each gripper arm inspired by the shape of the octopus tentacle. They are made from a soft silicone elastomer, which is structured to control the bending direction using pneumatic methods of actuation. The octopus-like tentacles of the OctopusGripper also contain suction abilities that can sustain a large gripping force with a working pressure of 2 bar [4]. A fully soft robot inspired by the octopus was presented by Fras et al [5], seen in Figure S1(c). With arms made with a novel soft fluidic actuator capable of manipulation as well as movement such as turning and forward propulsion. The robot is completely soft with even the main body being composed of an elastomer.

Calisti et al [6] has developed an octopus bio inspired robot. The prototype presented contains a silicone arm with embedded cables that were actuated by servo motors to mimic the bending of the biological octopus tentacle. They have demonstrated the use of the arm by grasping objects and a pushing-based locomotion. Moreover, they have demonstrated the control of the arm stiffness by coiling and uncoiling of an embedded steel cable in the arm.

Additionally, a multi-arm wirelessly controlled swimming octopus robot is presented [7,8,1,9], shown in Figure S1(d). This robot was able to propel itself and swim underwater at a speed of 0.26 body length/second driven by water-proof micro servomotors. It is also able to perform a turning maneuver using a sequence of actuation steps. The main body enclosure contains an empty cavity that can be filled with water which is utilized to control the buoyancy of the robot. Moreover, a soft robotic arm inspired by octopus arm embedded with coiled SMAs is presented. The arm can bend and manipulate to grasp objects, shown in Figure S1(e). The arm is made of transverse coiled SMA muscles around the cylinder shape of the octopus arm [10,11]. An 8-arm octopus like robot was fabricated and is seen in Figure S1(f). This robot has 8 soft silicone arms and a rigid central housing for the controlling unit. The robot presented with a buoyancy of almost neutral is shown to be able to move underwater over different surfaces and physical constraints. It is also able to grasp objects of different shapes and sizes. The swimming and grasping are a result of using two different arm actuating units. The motor crank is used for locomotion and the coiled SMA technology for manipulation [12].

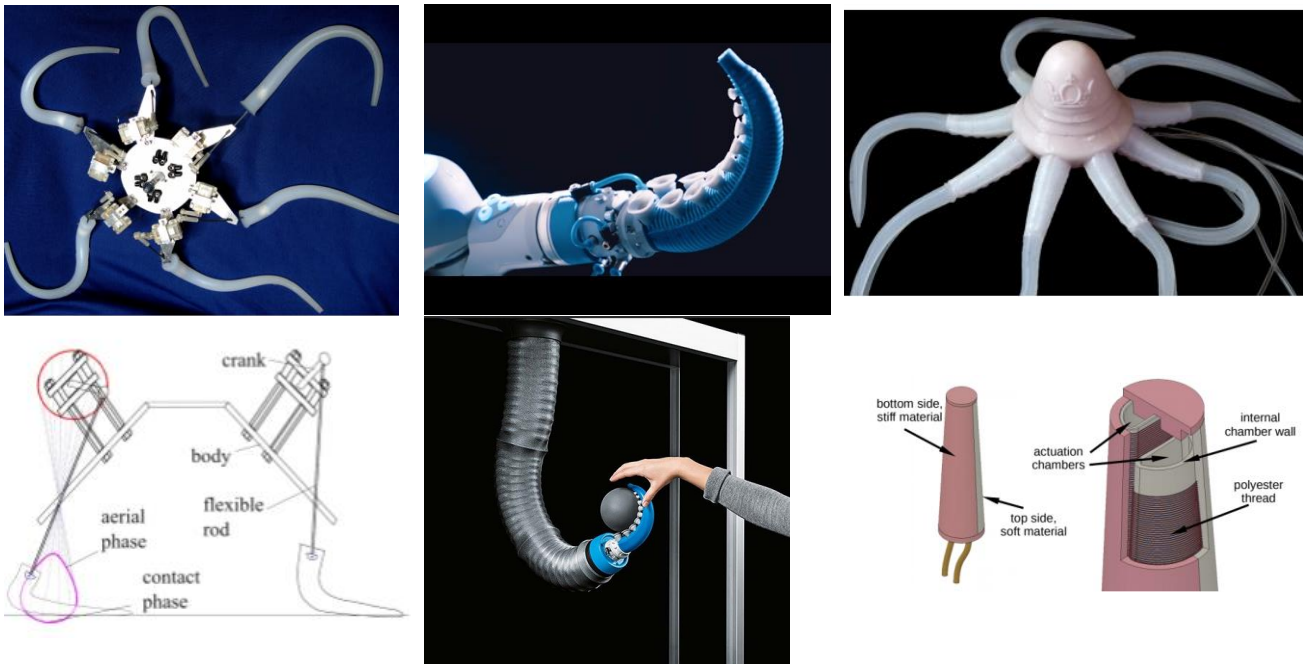

Fig. S1: Examples of octopus-like robot presented in the literature (a) PoseiDrone. (b)Octopus gripper (c) Fras et al fluidic bioinspired octopus robot [5] (d) multi-arm SMA swimming octopus robot (e) SMA actuated robot arm and transverse SMA actuators embedded in the robotic arm (f) Eight arm octopus robot

Actuation circuit used in isotonic testing for actuator characterization

Figure S2(a) shows the full experimental set up for actuator characterization. The set up contains a laser displacement sensor, thermocouples, calibrated weights, a power supply, NI 9221 to measure voltage, NI 9219 to measure temperature change using the thermocouples, and a laptop for measuring and saving the data using a programable LabView program. The NI 9221 voltage measurement device has a limitation of measuring up to 60V (max). Since the TCP_{FL} muscles have high resistance depending on the length, the voltage needed for testing is more than 60V. A voltage divider circuit is introduced to measure the voltage through a constant known current and then use equation (S1) to calculate the actual output voltage of the actuator.

$$V_{TCP} = \left(\frac{V_1}{R_1}\right) \times (R_1 + R_{TCP}) \quad \textbf{(S1)}$$

Where V_{TCP} and R_{TCP} are the actuator voltage and resistance consecutively, R_1 and V_1 are the known resistance and voltage across that resistor.

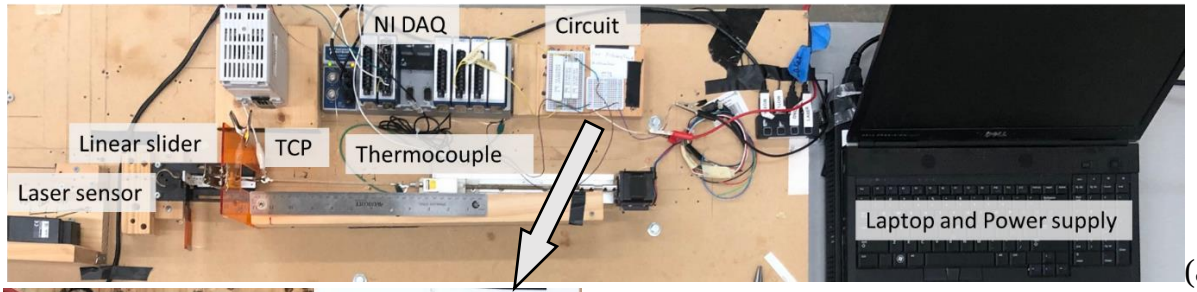

(a)

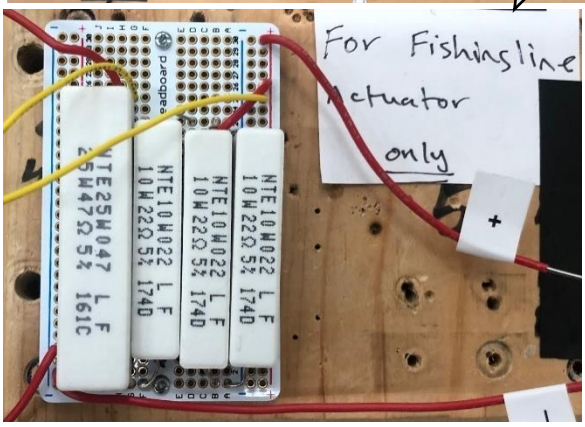

(b)

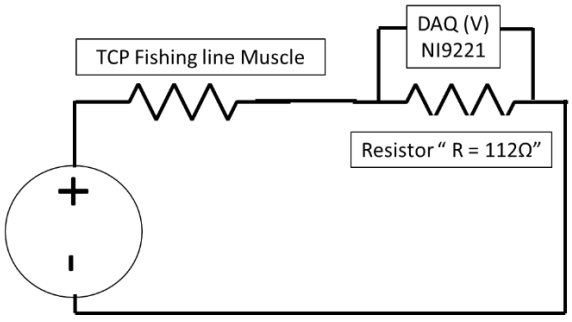

(c)

Fig. S2: Isotonic test set up circuit diagram (a) Snapshot of the experimental set up, (b) Close up snapshot of the voltage divider circuit, and (c) Schematics of the voltage divider circuit.

Schematic diagram of experimental set up for TCP_{FL} actuated arm

The experimental set up shown in Figure S3 explains the test set up for the TCP_{FL} in both air, Figure S3 (a), and in underwater, Figure S3 (b). In the case for the air set up, the arm structure is left suspended and the main body is fixed to a clamp. On the other hand, in the water set up, the arms are suspended inside the 70 gallon fish tank while the main body is fixed to the tank. In both cases a camera is used to capture videos and photos to quantify the data, while the power supply is directly connected to the TCP_{FL} actuator by copper wires to provide actuating power.

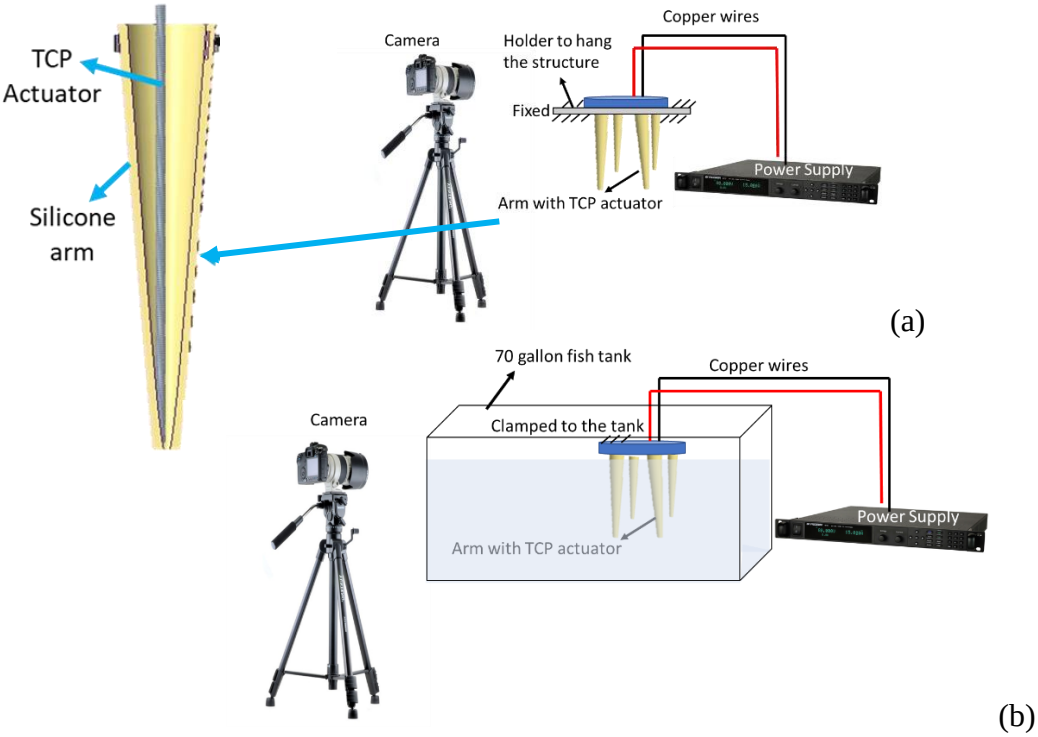

Fig. S3: Experimental set up (a) Testing in air environment (b) Testing underwater using a fish tank.

Stress analysis on 3D printed structure

The integrity of the cage was validated using a finite element analysis performed in Creo Parametric 4.0. The setup for the analysis required a few assumptions to be made. The objective of the analysis was to determine first whether the robot would be structurally safe at various depths. The water pressure P_{Water} is calculated in equation S2 according to the density of the water ρ, height h, and gravity g.

$$P_{Water} = \rho g h \quad \textbf{(S2)}$$

The difference in height of the robots highest and lowest points was not considered to be significant. The bottom surface of the cage was assumed to be set fixed to a stationary tank or ocean floor. This was reflected in the analysis by restricting all displacement on the lower surface of the cage. The material of the cage was ABSplus-P430.The different platforms are intended for different purposes; however, what is important for the validation that the design will work is

whether the platform will be able to stand up to the forces of the actuator, the components, and the water pressure, which will act on the cage and in turn on the platforms inside the cage. The results of the simulation conducted on the cage at different test depths are shown in Figure S4. The depths and data results are shown in Figure S4 (g), which include the test at 25, 50 and 100 feet. The 100 ft. test was also conducted on a carbon fiber cage to experiment with different materials compositions. The simulation revealed the high stress areas along the circular wall of the robot, something already anticipated due to the thin outer and inner walls of the robot that were designed to give a hollow cavity inside of the cage, wherein more weight could be added. At a depth of 25 feet (Figure S4(a)), the simulation indicated low deformation areas at the 50 and 100 feet. Figures S4(b-c) showed high deformation along the circular walls of the cage.

We determined that the extrusions of the platform are the most likely failing point due to the stress they will experience from the water pressure on the cage, as well as their shape, which contains sharp corners and is more viable to stress concentrations. While there would be forces on the actual platform itself, these would primarily come from the weight of the components inside and from the reaction forces of the actuation at the connections. To simulate this situation, force simulations were performed on the protruding lip of the disks, that meet the cage, wherein the pressure on the protruding lip was the same as the pressure would be on the cage. The platforms were made of a polymer known as ABS M30. The material properties in the simulation are the same for the platforms and what we analyzed for the extrusions is not just the Von Mises stress but whether the displacement and the stress at the extrusions is enough to cause any problems with the sealing material, which will be placed on the bottom disk to cause the seal to break. We looked at two things, the first being the deformation and the second being the Von Mises stress. Both of these have an underwater pressure of 2.6 psi plus the atmospheric pressure of 14.69 psi. Both of them fell well below the upper bounds of the ABS material at 32 psi max and 1.47E-05 inches for the deformation for the test depth of 6ft. According to these calculations, as long as the seal is sound, the deformation of the plastic will not cause any issues with the seal when the depth is at 6 feet. The results for the deformation and pressure at 25, 50, and 100 feet of depth in figure S4 (g) showed a linear relationship between the deformation and the depth. The point of failure appeared between 25 and 50 feet, wherein the stress and deformation exceeded the limit, the previously mentioned upper bounds of 32psi, for the ABS M30 polymer.

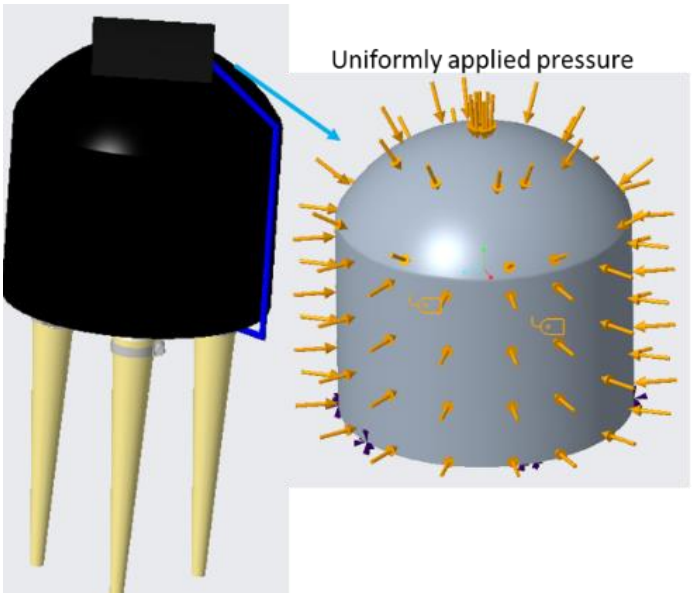

(a)

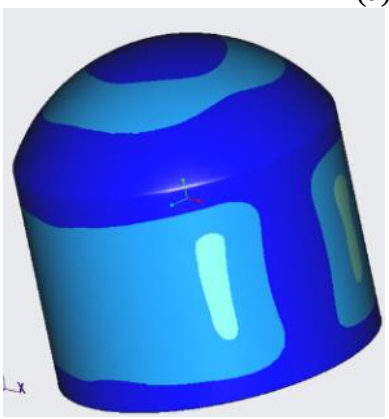

(b)

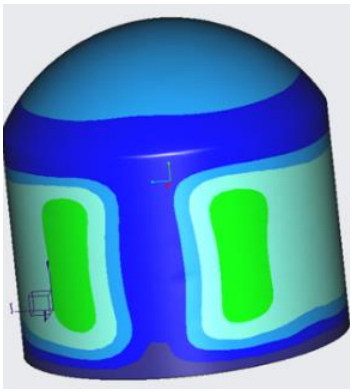

(c)

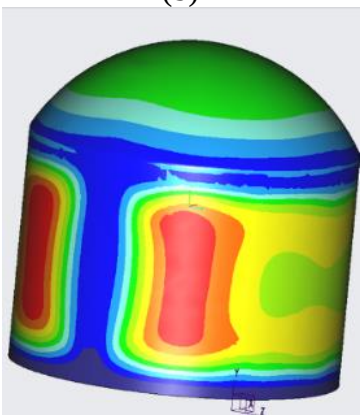

(d)

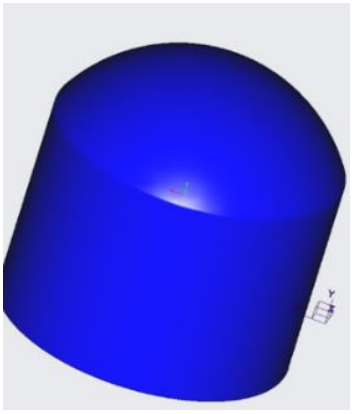

(e)

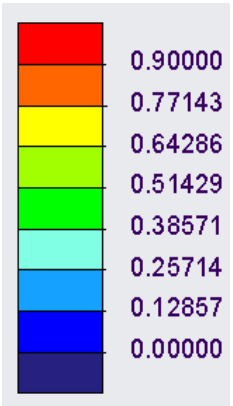

(f)

Material	Depth in sea water (ft)	Pressure (atm)	Max Stress (MPa)	Max Displacement (mm)
ABS Plastic	25	0.76	15.2	0.23
ABS Plastic	50	1.53	30	0.48
ABS Plastic	100	3.02	60	0.94
Carbon Fiber	100	3.02	60	0.039

(g)

Fig. S4: Deformation simulation using finite element analysis at depth and pressure of (a) applied uniform pressure on the structure, (b) ABS plastic at 25ft water depth , P = 0.76 atm, (c) ABS plastic at 50 ft, P = 1.53 atm, (d) ABS plastic at 100ft, P = 3.02 atm, (e) Carbon fiber at 100 ft, P = 3.02atm, and (f) Contour color legend of the deformed values (mm). (g) Simulation parameters and numerical results

Fabrication of fishing line muscle with thin heating wire

The fabrication of the self-coiled fishing line muscle (properties are shown in Table S1) with heating element is simple, scalable, and easy to follow which allows for in house manufacturing of the actuators at low cost. It consists of four major steps following Wu et al [13] and shown in movie 7, explained in Figure S5[13]. First, twist insertion; second, wrapping of nichrome resistance wire; third, coiling; and fourth, thermal annealing and training. The fabrication set up includes two stepper motors (MT1 and MT2) to control the twisting, resistance wire wrapping, and coiling. The setup also includes a guide rod and calibrated weights to keep the precursor fiber in tension. The fabrication process starts by attaching the precursor fiber of fishing line muscle, purchased from eagle claw fishing line (d = 0.8 mm, L = 1143 mm), to MT1 on one end and 500g deadweight connected with a stopper on the other end. MT1 runs counterclockwise introducing an initial twist to the precursor fiber.

After the nichrome wire is fully incorporated, the stopper rod is added to the bottom end of the muscle again and MT1 is activated to start the coiling process. Once the muscle is fully coiled, it is crimped on both ends and annealed in a furnace at 180°C for 90 minutes to preserve its coiled shape. This annealing process aligns the crystal structure of the nylon, which allows it to stay at the coiled shape. Lastly, the muscle is trained at 300g load at the following cycles shown in Figure 5 (c) to retain a certain actuation load.

Annealing and training of self-coiled fishing line actuator

After the mechanical process, the actuator is placed in a 180 ^{0}C furnace for 90 minutes for annealing. The annealing process allows the actuator to permanently retain its coiled shape. Training is then performed. It is observed that the muscle initially required training at lower currents and short heating time while gradually increasing it. The muscle is considered fully trained when steady state actuation strain is observed. Table S1 shows the training parameters used for the self-coiled fishing line actuator.

(a)

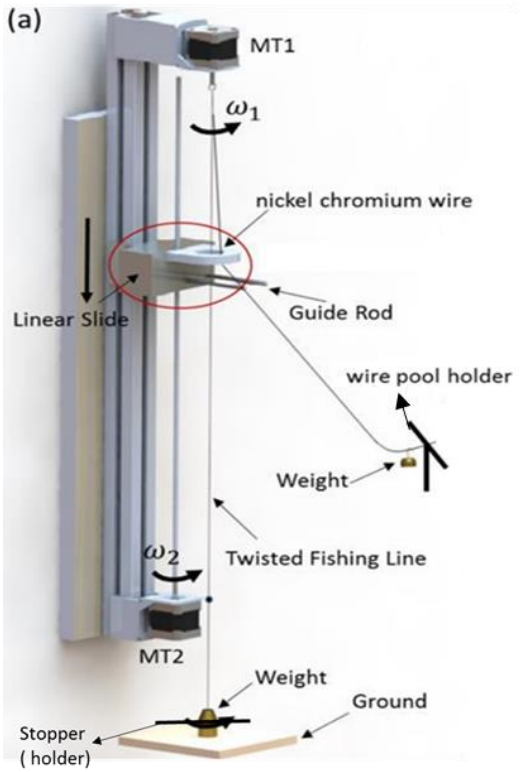

(b)

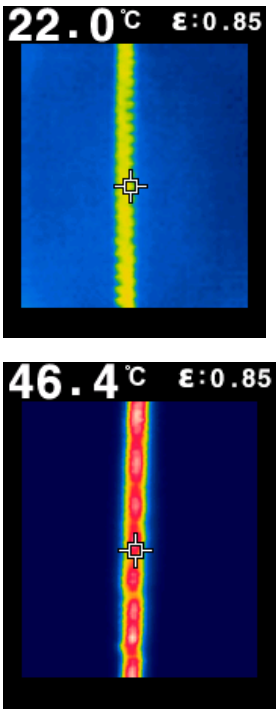

(c)

Step 1		
Heating time (s)	5	Repeating
Cooling time (s)	60	5
Input Current (A) should be kept at open voltage	0.12	
Step 2		
Heating time (s)	10	10
Cooling time (s)	60	
Input Current (A) should be kept at open voltage	0.12	
Step 3		
Heating time (s)	10	10
Cooling time (s)	80	
Input Current (A) should be kept at open voltage	0.14	
Step 4		
Heating time (s)	15	15
Cooling time (s)	80	
Input Current (A) should be kept at open voltage	0.14	

Fig. S5: Self coiled fishing line fabrication and specifications. fishing line fabrication process precursor diameter "d" = 0.8mm. (b) Thermal imaging of $TCP_{FL.}$ Top is before actuation and bottom is during actuation. Actuation information are location in Table S1. (c) Training parameters for self-coiled fishing line actuator

Table S1: Fishing line TCP actuator information

Material	Nylon (6,6) fishing line
Type of actuation	Electrothermal
Type of resistance wire	Nichrome (nickel, chromium)
Resistance wire diameter	d_w=80 µm
Precursor fiber diameter	d =0.8 mm
Length of precursor fiber	l = 1143 mm
Weight for fabrication	m_f = 500 g
Annealing Temperature/ Time	Ta=180^{0}C/ 90 min
Training protocol	According to figure 5 (c)
Diameter after coiling	D=2.8mm
Length after coiling	L=110 mm
Resistance	R= 256Ω
Current (Input)	I= 0.14A - 0.47A
Voltage (across the actuator)	V= 35V - 120V
Actuation input power (V*I)	P = 4.9W - 56.4W
Heating time(t_h)	t_h=25s - 1s
Cooling time (t_c)	t_c =100s - 9s
Heating energy (V*I*t_h)	E_h=122.5J - 56.4J
Actuation frequency	f = 8mHz – 0.1Hz
Actuation strain, at 300g load	ε = 40% - 10% @3N load

Overall robot design (mechanical and electrical components)

The connectivity diagram in Figure S6(a) shows the schematics of all the mechanical and electrical components of the robot. The robot is divided into three levels. The first level contains the four 5.5 kg-cm bipolar NEMA 17 stepper motors and the TCP_{FL} that control the soft silicone arm. The second level contains the buoyancy system, which is comprised of two solenoid valves, check valve, pressure regulator, air bladder, and a 16g CO_2 canister. Lastly, the third level contains the electrical controlling circuit. These three levels are stacked on top of each other and housed within a 3D printed plastic shell. Figure S7(b-d) show the assembled octopus robot before and while deployment during underwater testing.

Level 1 shown in Figure S7 (b) contains the four stepper motors. Each motor has its own motor driver and the motor is connected to a tendon that is embedded in the silicone arm at one end. The motors are wirelessly controlled by a joystick, and when activated, the motor will coil the tendon on its shaft allowing the arm to bend and rotate to grab objects underwater. The other actuation method of the arm uses the contraction of the TCP_{FL} and move the silicone arm. The TCP_{FL} can be directly connected to the battery through a GEREE 250W Boost Converter. This converter takes the 8.5 - 48V DC to 12-50V DC output by stepping-up the battery power and it has a maximum current of 10A. This essentially uses capacitors to store up the voltage from the battery and increasing the initial voltage of 14.8V to a max of 50V to accommodate the voltage consumption of the TCP_{FL}.

Level 2 of the octopus robot contains the buoyancy system as shown in detail in Figure S7(b). A 16g CO_2 canister pressure is controlled by the pressure regulator. When the first solenoid valve is opened, the air bladder fills up, which helps the Kraken rise underwater. This solenoid valve is then closed, and the air remains within the bladder and maintain the robot's position at a particular height. The second solenoid valve opens and the air from the bladder rushes out of the robot through a tube the bottom of the first level platform of the robot. Both the solenoid valve and the pressure of the air bladder prevent water from flowing back into the air bladder, and only allows air to exit. This makes the robot to deflate the air bladder and return to its original position.

The third and final level contains the electrical components, which includes a battery power source, an Arduino board, and motor drivers. The overall sealing process is explained in Figure S7(c) which is one of the important processes for an underwater robot. A schematic diagram of the circuit connections is explained in Figure S8(a) that shows the mechatronic components. A wireless joystick controller, Figure S8(b), was programmed with commands to wirelessly control the robot up to 25ft. The program allows a user to select and activate each task at a time. The main menu selection starts by selecting between arms 1-4 or the buoyancy system. If an arm is chosen, the user can push up or down to actuate it to either grab or release an object. If the buoyancy system is chosen, the user can inflate or deflate the air bladder to control the vertical depth of the Kraken. A detailed schematic is shown in Figure S8(c) for the user operational software interface**.**

Kraken is weighed down with two different methods. The first method is by filling sand or other materials in the shelled 3D printed plastic casing. In our first test, the empty space within the components is filled with sand, specifically riverbed sand, to increase the weight of the robot. The

second method involves an anchor system. The anchor is a cast iron plate with nylon straps across the bottom and looping around the cage of the robot to evenly distribute the weight. Doing this will allow the robot to have better control in picking up an object that is not directly under it. Weighing down the Kraken underwater will allow for overall stability of the robot and the ability to get the robot as neutrally buoyant as possible.

Connectivity diagram of the robot's components

Figure S6(a) shows the robot's overall connectivity diagram. The octopus like robot is powered by a 14.8V Li-ion battery connected to the controller circuit which includes the motors, buoyancy system, sensor, and the wireless shield. The wireless Xbee is used to communicate with the joystick controlled by the user. Figure S6(b-d) shows the robot fully assembled before deployment, during deployment, and fully functioning underwater in a swimming pool consecutively.

(a)

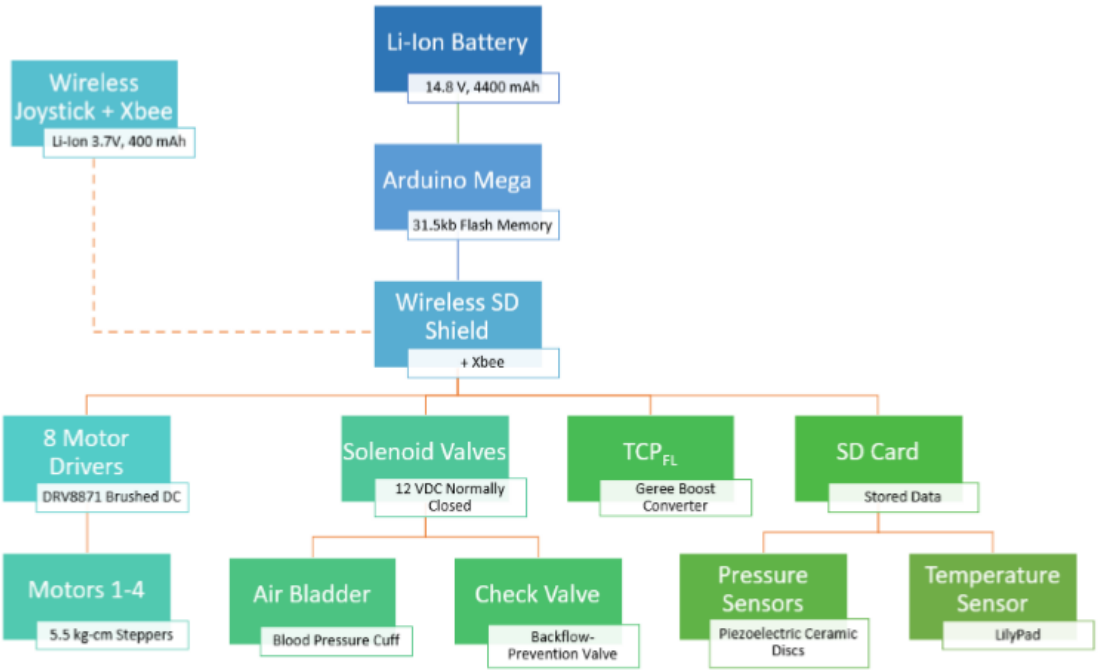

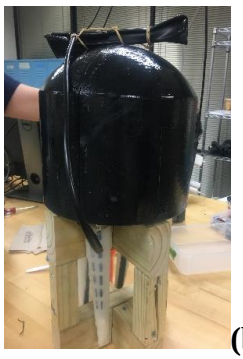

(b)

(c)

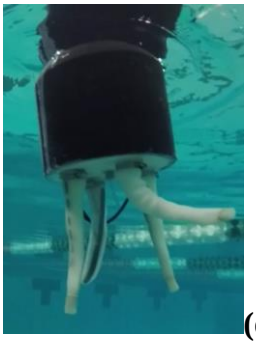

(d)

Fig. S6: Wiring diagram and preparing the robot for experiment: (a) Octopus components diagram, (b) photo of 3D printed octopus robot, (c) UTD students testing octopus underwater and (d) photo of underwater grasping.

Molding of silicone arm

A step by step process of creating one of the basic arms found on Kraken is presented in Figure S7(a). The process first starts out with the molding of the silicone arms. Using a flat 3D printed mold of the arm shape. Mann Ease Release 200 spray was applied throughout the surface of the mold to prevent sticking. EcoFlex 00-30 part A and B were mixed together at a 1:1 ratio and a small layer of silicone was poured into the mold. Silicone elastomer material (Ecoflex-0030) is used as an artificial skin material due to its elasticity and molding abilities. After mixing the silicone, the chosen arrangement of spring steels is added to the first layer of silicone. The specific arrangement and thickness of the spring steels will determine the shape the arm takes when actuated. This was explained previously in Figure 2 in the main paper. Adding thin strips as shown in Figure 2(a-b) will cause the arm to bend at different axes, while adding one long strip such as what is shown in Figure 2 (c-f) will cause bending on one axis. Also, depending on the angle of orientation that the spring steel is embedded with, we can achieve different curling configurations. After laying out the desired configuration, the rest of the silicone is then poured on top of the spring steel layer. To connect the arm to the stepper motor, a long piece of fishing line passive structure (used as tendon) is embedded into the bottom end of the silicone while it is still uncured. Once the silicone is cured, it is removed from the mold. Then, beginning from the base of the arm, the silicone is folded over the sides and the cap is sealed using small amounts of fast curing EcoFlex 00-35. Moreover, cotton was added inside the arm to increase the stiffness. A similar process is also implemented for the TCP_{FL} arm by placing the coiled fishing line muscle instead of the passive fiber before curing and folding the silicone.

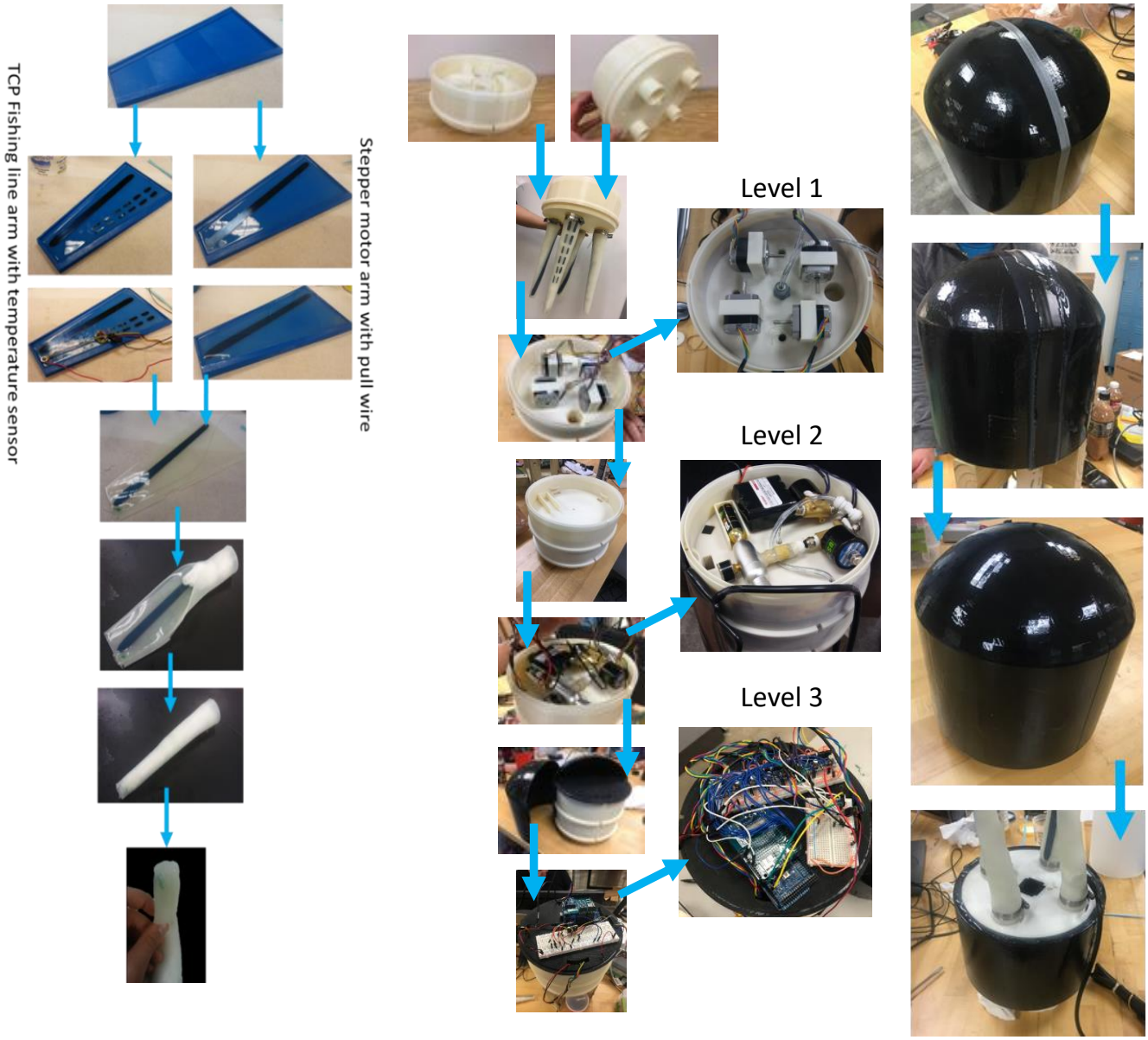

Fig. S7: Fabrication process (a) Silicone arm fabrication process, (b) 3D printed parts assembly, detailed view of the three internal levels, level 1stepper motors, level 2 buoyancy system, level 3 electrical circuit. (c) Water sealing process using FlexSeal paint.

Robot controlling circuit

A full circuit diagram is shown in Figure S8(a). A detailed schematic of the joystick controller and options is found in Figure S8(b and c). Here, the user is able to select from a menu to either control one of the four arms (arms 1-4 and TCP) and the buoyancy system (bladder). After selecting the component to activate, the user can then select to move the arm (up or down) or inflate or deflate the air bladder for vertical swimming.

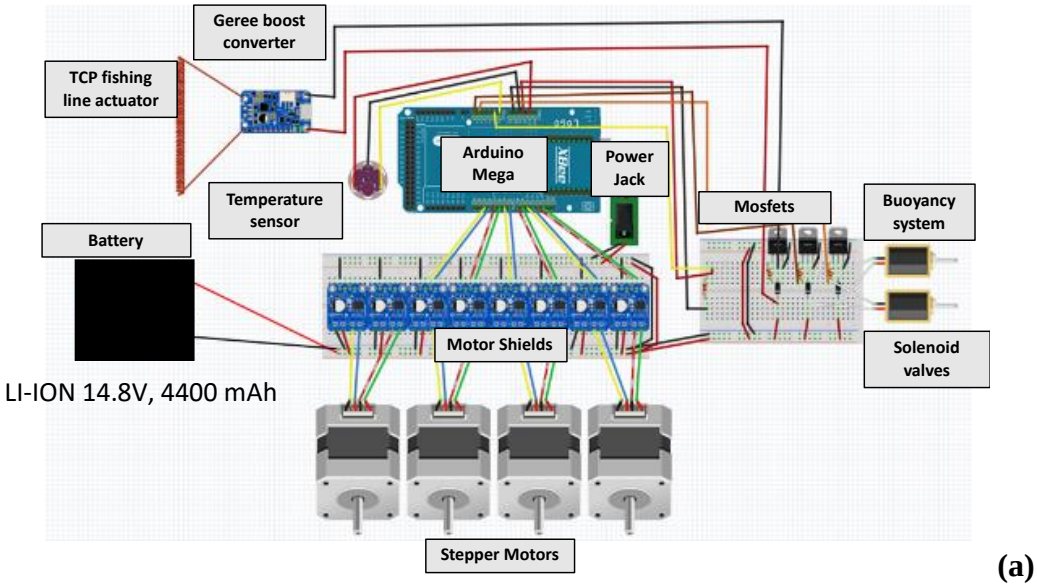

(a)

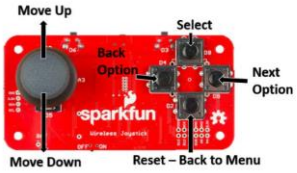

(b)

(c)

Fig. S8: (a) Schematic diagram of electrical circuit, (b) Wireless joystick, and (c) Programed controlling menu command.

ANSYS Fluent Simulation Setup

For flow analysis, the CAD file created in SolidWorks is imported into ANSYS DesignModeler. A cuboidal domain with dimensions 80 x 40 x 100 in^3 (Figure S9 (a)), is created around the main body. A cylindrical enclosure surrounding the model is created for the purpose of meshing and applying uniform motion. A Boolean operation is implemented to subtract the solid model from the fluid domain. Figure S9 shows the computational domain geometry. The domain is meshed with tetrahedral elements of size 1 in. with a finer size of 0.25 in. inside the cylindrical zone created around the model. Five inflation layers (prism layers) surround the model to capture the boundary layer as shown in Figure S9(b). The analysis is a transient incompressible flow analysis. The models chosen for this simulation are Viscous $\rightarrow k-\varepsilon$ Turbulence Model $\rightarrow$ Realizable with Scalable Wall Functions. The fluid is selected as water, which is available in the Fluent database. The dynamic mesh model is activated for this simulation. A diffusion based smoothing method is used with a diffusion parameter of 0.7, which would not affect the mesh very far away from the body. A local cell and region face remeshing method is applied in addition to smoothing with the domain mesh scale parameters. The remeshing algorithm is implemented every 2 time-steps to ensure that the mesh does not become very distorted due to the motion of the body. The motion for the model is assigned by importing and compiling a user defined function (UDF) for the six DOF solver. A snippet of the UDF is shown in Figure S9 (c). In the calculation parameters, the time-step is chosen to be 0.001 seconds and each time-step goes through a maximum of 80 iterations to achieve proper convergence within a time-step.

Flow Simulation

An underwater flow simulation study of the vertical motion of the Kraken is studied using ANSYS Fluent (v17.0) software. Yue et. al [14] suggest simplifying the 3D model so as to reduce the computational time and get more effective results for such kind of underwater studies. Since the model is sealed completely, all the internal structures are removed by generating the model as a solid body. A cuboidal fluid domain is generated around the model, the sides of which are at 4 times the diameter of the cage and the vertical height is 5 times the total length of the model. These lengths are chosen by assuming that they can act as far-field boundaries. The flow domain is generated by creating a Boolean operation to subtract the solid model from the flow field. A smaller cylindrical inner zone, which will move along with the model surrounds it to ensure uniform motion and lower risk of mesh distortion. Defining a proper mesh is the key to get accurate results while balancing the computational complexity. A tetrahedral dominant mesh with around 0.1 million nodes and 0.5 million elements captures the motion and the flow field as a result of it. The mesh around the Kraken is dense compared to the rest of the domain in order to precisely predict the flow field around the model shown in Figure S9 (b). 5 prism layers which run parallel to the surface topology are generated around the Kraken to capture the boundary layer.

The flow field resulting from the motion of Kraken is calculated by the unsteady incompressible Reynolds-averaged Navier Stokes (RANS) equations as shown in equations S3 and S4:

$$\frac{\partial u_j}{\partial x_j} = 0 \qquad \text{(S3)}$$

$$\frac{\partial u_i}{\partial t} + \frac{\partial u_i u_j}{\partial x_j} = -\frac{1}{\rho}\frac{\partial P}{\partial x_i} + \nu\frac{\partial}{\partial x_j}\left[\left(\frac{\partial u_i}{\partial x_j} + \frac{\partial u_j}{\partial x_i}\right)\right] - \frac{\partial \overline{u_i' u_j'}}{\partial x_j} \quad \text{(S4)}$$

where u_i and u_i' are the mean and fluctuating components of the instantaneous velocity, P is the mean component of instantaneous pressure and ν is the kinematic viscosity

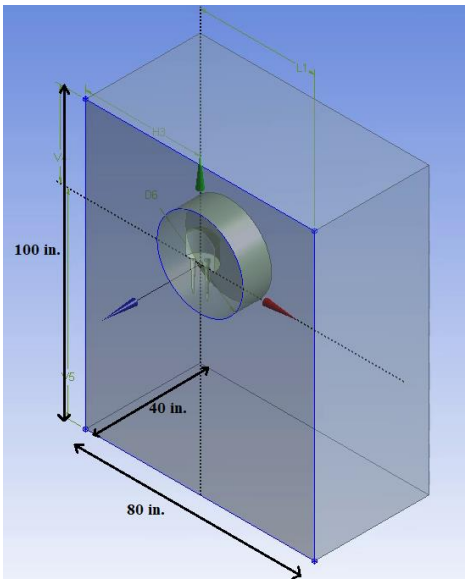

(a)

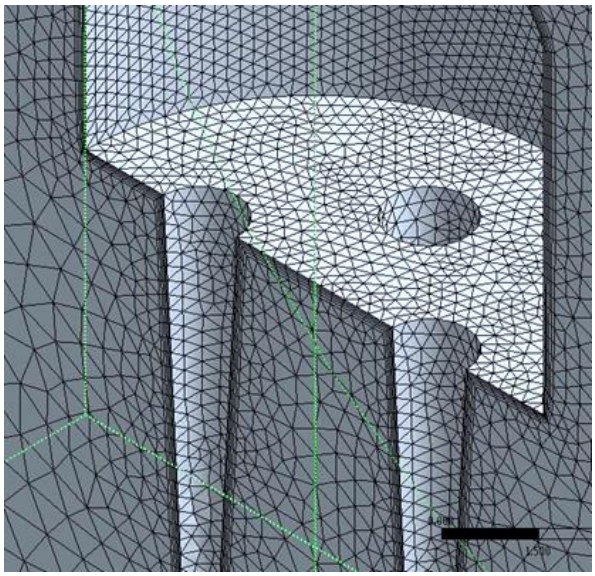

(b)

DynamicMesh - Notepad

File Edit Format View Help

```
#include "udf.h"

DEFINE_SDOF_PROPERTIES(octopus_body, prop, dt, time, dtime)
{
        prop[SDOF_MASS] = 14.2934;
}

DEFINE_CG_MOTION(octopus, dt, vel, omega, time, dtime)
{
        real current_time;
        current_time = CURRENT_TIME;
        vel[0] = 0.0;
        vel[1] = -0.0198*current_time;
        vel[2] = 0.0;

        omega[0] = 0.0;
        omega[1] = 0.0;
        omega[2] = 0.0;
}
```

(c)

Fig.S9: (a) Computational domain of interest for the flow simulation. (b) Meshed computational domain in the vicinity of the model. (c) A snippet of the user defined function (UDF) used for assigning the motion of the model

. The realizable k- ε turbulence model with scalable wall functions solver is used to study the dynamics of the fluid domain. This turbulence model can provide accurate and superior performance in flows involving recirculation [15]. The model is split vertically in half in order to dimensionally reduce the domain. The mid-plane is assigned the symmetry boundary conditions while the sides of the domain are assigned as walls. The pressure is assumed constant throughout the domain because of the relatively small difference in vertical height. In order to impart the motion, a user-defined function is compiled in Fluent. The user-defined function consists of the

physical properties of the robot, such as the mass as well as the motion parameters, such as linear and angular velocity. The surface of Kraken is assigned the wall boundary condition as shown in equation S5 which propagates the motion from the Kraken to the surrounding fluid domain.

$$U - U_{wall} = 0 \quad \textbf{(S5)}$$

For this study, the simulation is done by moving the model vertically upwards with a velocity of 1 m/s, giving it a Reynolds' number of around 5.7e5 for the first part and letting it sink under acceleration of 0.0198 m/s^2 calculated from the experiment (time-dependent velocity) for the second part. The upward velocity was chosen considering the fact that an octopus can propel as fast as 40 km/h (11.11 m/s) upwards. Hence a high velocity of swimming (1 m/s) is chosen as a test value. For the sinking part, a more realistic model-based value of acceleration is implemented. Two methods can be used to define the interaction between the model and the fluid: (a) dynamic meshing, which sets the fluid as stationary and the model to move, and (b) fluid moving in the opposite direction as the model, which mimics the relative motion between the two [14]. Both these methods were analyzed by Leong et al. [16] who concluded that the results provided by both of them are just marginally different from the experimental results. For this study, a dynamic meshing approach has been chosen with smoothing, re-meshing and six DOF rigid body motion solver so as to accurately replicate the phenomenon. The time step is chosen in a way such that the displacement of the Kraken in a single time step is less than half the mesh size to avoid any negative volume error that might occur due to the mesh motion. This ensures that the dynamic mesh is able to properly smoothen and re-mesh before the next time step. The first simulation (rising up) is executed for 1 sec and the second simulation, which replicates our experiment in the swimming pool is performed for 8 sec.

References

1. Sfakiotakis, M., Kazakidi, A., Pateromichelakis, N., Tsakiris, D.P.: Octopus-inspired eight-arm robotic swimming by sculling movements. In: Robotics and Automation (ICRA), 2013 IEEE International Conference on 2013, pp. 5155-5161. IEEE
2. Arienti, A., Calisti, M., Giorgio-Serchi, F., Laschi, C.: PoseiDRONE: design of a soft-bodied ROV with crawling, swimming and manipulation ability. In: Oceans-San Diego, 2013 2013, pp. 1-7. IEEE
3. Serchi, F.G., Arienti, A., Laschi, C.: Biomimetic vortex propulsion: toward the new paradigm of soft unmanned underwater vehicles. IEEE/ASME Transactions On Mechatronics **18**(2), 484-493 (2013).
4. Festo: OctopusGripper and BionicCobot (undated). https://www.festo.com/group/en/cms/12745.htm
5. Fras, J., Noh, Y., Macias, M., Wurdemann, H., Althoefer, K.: Bio-inspired octopus robot based on novel soft fluidic actuator. In: 2018 IEEE International Conference on Robotics and Automation (ICRA) 2018, pp. 1583-1588. IEEE
6. Calisti, M., Giorelli, M., Levy, G., Mazzolai, B., Hochner, B., Laschi, C., Dario, P.: An octopus-bioinspired solution to movement and manipulation for soft robots. Bioinspiration & biomimetics **6**(3), 036002 (2011).
7. Sfakiotakis, M., Kazakidi, A., Tsakiris, D.P.: Turning maneuvers of an octopus-inspired multi-arm robotic swimmer. In: Control & Automation (MED), 2013 21st Mediterranean Conference on 2013, pp. 1343-1349. IEEE
8. Sfakiotakis, M., Kazakidi, A., Tsakiris, D.: Octopus-inspired multi-arm robotic swimming. Bioinspiration & biomimetics **10**(3), 035005 (2015).
9. Sfakiotakis, M., Kazakidi, A., Chatzidaki, A., Evdaimon, T., Tsakiris, D.P.: Multi-arm robotic swimming with octopus-inspired compliant web. In: Intelligent Robots and Systems (IROS 2014), 2014 IEEE/RSJ International Conference on 2014, pp. 302-308. IEEE
10. Laschi, C., Cianchetti, M., Mazzolai, B., Margheri, L., Follador, M., Dario, P.: Soft robot arm inspired by the octopus. Advanced Robotics **26**(7), 709-727 (2012).
11. Mazzolai, B., Margheri, L., Cianchetti, M., Dario, P., Laschi, C.: Soft-robotic arm inspired by the octopus: II. From artificial requirements to innovative technological solutions. Bioinspiration & biomimetics **7**(2), 025005 (2012).
12. Cianchetti, M., Calisti, M., Margheri, L., Kuba, M., Laschi, C.: Bioinspired locomotion and grasping in water: the soft eight-arm OCTOPUS robot. Bioinspiration & biomimetics **10**(3), 035003 (2015).
13. Wu, L., Chauhan, I., Tadesse, Y.: A Novel Soft Actuator for the Musculoskeletal System. Advanced Materials Technologies **3**(5), 1700359 (2018).
14. Yue, C., Guo, S., Li, M.: ANSYS FLUENT-based modeling and hydrodynamic analysis for a spherical underwater robot. In: Mechatronics and Automation (ICMA), 2013 IEEE International Conference on 2013, pp. 1577-1581. IEEE
15. ANSYS.Inc.
16. Leong, Z.Q., Ranmuthugala, D., Penesis, I., Nguyen, H.D.: Computational fluid dynamics re-mesh method to generating hydrodynamic models for maneuvering simulation of two submerged bodies in relative motion. Journal of Computer Science and Cybernetics **27**(4), 353-362 (2011).